Removal of endosulfan from water by municipal waste incineration fly ash-based geopolymers: Adsorption kinetics, isotherms, and thermodynamics

Article · March 2023

DOI: 10.3389/fenvc.2023.1164372

5 authors, including:

Daniel Onunga
University of KwaZulu-Natal
9 PUBLICATIONS **34** CITATIONS
SEE PROFILE

Victor Shikuku
Kaimosi Friends University
55 PUBLICATIONS **495** CITATIONS
SEE PROFILE

Benton Otieno
Vaal University of Technology
25 PUBLICATIONS **208** CITATIONS
SEE PROFILE

Kowenje Chrispin
Maseno University
52 PUBLICATIONS **515** CITATIONS
SEE PROFILE

frontiers | Frontiers in Environmental Chemistry

TYPE Original Research
PUBLISHED 23 March 2023
DOI 10.3389/fenvc.2023.1164372

OPEN ACCESS

EDITED BY
Mohamed Zbair,
UMR7361 Institut de Sciences des Matériaux de Mulhouse, France

REVIEWED BY
Asma Amjlef,
Ibn Zohr University, Morocco
Aprilina Purbasari,
Diponegoro University, Indonesia

*CORRESPONDENCE
Victor O. Shikuku,
vshikuku@kafu.ac.ke

SPECIALTY SECTION
This article was submitted to Sorption Technologies, a section of the journal Frontiers in Environmental Chemistry

RECEIVED 12 February 2023
ACCEPTED 08 March 2023
PUBLISHED 23 March 2023

CITATION
Luttah I, Onunga DO, Shikuku VO, Otieno B and Kowenje CO (2023), Removal of endosulfan from water by municipal waste incineration fly ash-based geopolymers: Adsorption kinetics, isotherms, and thermodynamics. *Front. Environ. Chem.* 4:1164372. doi: 10.3389/fenvc.2023.1164372

Removal of endosulfan from water by municipal waste incineration fly ash-based geopolymers: Adsorption kinetics, isotherms, and thermodynamics

Isaac Luttah[1], Daniel O. Onunga[1], Victor O. Shikuku[2]*, Benton Otieno[3] and Chrispin O. Kowenje[1]

[1]Department of Chemistry, Faculty of Physical and Biological Sciences, Maseno University, Kisumu, Kenya, [2]Department of Physical Sciences, Kaimosi Friends University, Kaimosi, Kenya, [3]Department of Chemical and Metallurgical Engineering, Vaal University of Technology, Vanderbijlpark, South Africa

Alkali-activated municipal waste incineration fly ash (MWFA)-based geopolymers (GPA, GPB, and GPC) were synthesized under different sodium silicate to sodium hydroxide (SS/SH) ratios. The geopolymers were applied in the removal of endosulfan, a persistent and toxic chemical, from water. The adsorbents were characterized by XRD, SEM-EDX, and FTIR. Variation of SS/SH ratios resulted in morphologically distinguishable geopolymers with different compositions. The adsorption equilibrium data were best described by the Langmuir isotherm. The maximum adsorption capacities increased with an increase in SS/SH ratios in the order 1.87, 15.89, 16.97, and 20.01 mg/g for MWFA, GPA, GPB, and GPC, respectively. The kinetic data were best described by the *pseudo*-first-order model wherein the adsorption rate (k_1) was independent of the SS/SH ratios and the geopolymer composition. The thermodynamic parameters, that is, enthalpy ($\Delta H > 0$), Gibbs free energy ($\Delta G < 0$), entropy ($\Delta S > 0$), and activation energy ($E_a > 0$), show that the processes were endothermic, spontaneous, physical (E_a and $\Delta H < 40$ kJ/mol), and entropy-driven. Alkalination was beneficial since the geopolymers had a higher adsorption capacity (~8–10 times) and affinity for endosulfan (~30 times) than the precursor material (MWFA). The adsorption mechanism entailed electrostatic interactions and hydrogen bonding. The MWFA-based geopolymers are, therefore, potential alternative low-cost adsorbents for the removal of endosulfan from water and a strategy for the valorization of MWFA.

KEYWORDS

municipal waste incineration fly ash, geopolymer, endosulfan, adsorption, water

1 Introduction

Insecticides are pesticides formulated to kill, harm, repel, or mitigate one or more species of insects through different mechanisms such as disrupting the nervous system, damaging their exoskeletons, repelling them, or controlling them by interfering with their genetics and reproduction (Kegley et al., 2010). Insecticides include ovicides and larvicides applied against target insect eggs and larvae. The application of insecticides in plantations leads to increased

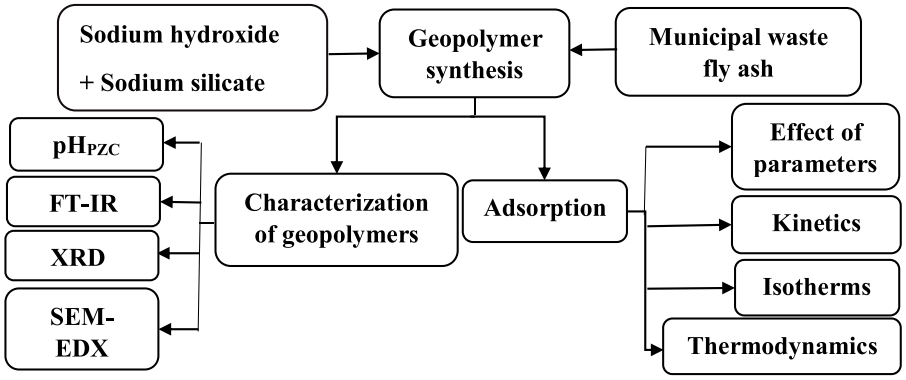

GRAPHICAL ABSTRACT

yields (Kughur, 2012). However, extensive and uncontrolled use of such agrochemicals leads to water pollution (Al-Samarai et al., 2018).

Endosulfan (6,9-methano-2,4,3-benzodioxathiepin,6,7,8,9,10,10-hexachloro-1,5,5a,6,9,9a-hexahydro-3,3-dioxide) is a broad-spectrum organochlorine insecticide of the cyclodiene subgroup which acts as a contact poison in a wide variety of insects. Most organochlorides act on neurons by causing a sodium/potassium imbalance preventing normal transmission of nerve impulses. Some act on the gamma-aminobutyric acid (GABA) receptor preventing chloride ions from entering the neurons, causing a hyperexcitable state characterized by tremors and convulsions. Endosulfan, for example, is a GABA-gated chloride channel antagonist (Sipes et al., 2013). For this reason, endosulfan and most other broad-spectrum insecticides have been eliminated (Lubick, 2010). Like most agrochemicals, endosulfan finds its way to water sources either through leaching, uncontrolled dumping of used endosulfan containers, the release of untreated industrial effluents, surface run-off, and farmyard deposition (Hwang et al., 2018).

Endosulfan is known to cause teratogenic malformations in fish and amphibians by disrupting hormones in frogs, cause ecological disturbance in freshwater ecosystems through alteration in the composition of planktonic algae species, and lead to death of aquatic animals (Lubick, 2010; Patocka et al., 2016). According to Roberts et al. (2007), maternal exposure to endosulfan during the first and second trimesters can lead to autism disorders. Due to its toxicity, the environmental fate of endosulfan is of great concern.

Conventionally, the activated carbon method has been used to remove water pollutants from contaminated water. For example, carbon slurry as a novel adsorbent material for the removal of endosulfan from contaminated water has been reported (Gupta and Imran, 2008; Kakoi et al., 2015). Hengpraprom et al. (2006) and Polati et al. (2006) reported the adsorption of *a*-endosulfan onto kaolinite particles and to a mixture of kaolinite and montmorillonite particles from aqueous suspension, respectively.

Similarly, studies on endosulfan adsorption onto hydrophobic HBEA zeolites (Yonli et al., 2012) and high-silica zeolites (Jiang et al., 2018) have been documented. These studies provide evidence of the suitability of aluminosilicate-based materials as adsorbents for endosulfan removal. Recently, geopolymers have shown to be emerging low-cost and efficient aluminosilicate adsorbents for the removal of various contaminants such as heavy metals and dyes from water, owing to a plethora of precursor materials available for geopolymer development (Shikuku et al., 2019). The materials evaluated for geopolymer development for water purification include metakaolin (Shikuku et al., 2022), volcanic ash (Tome et al., 2021), pozzolan and biochar composites (Dzoujo et al., 2022), and municipal solid waste incineration fly ash (Al-Ghouti et al., 2020) among others. For example, Craig et al. (2015) reported the application of biochar/geopolymer composites in the remediation of pesticides (such as atrazine, dieldrin, picloram, metolachlor, tebuthiuron, and hexazinone) from contaminated water. Albeit little research work has been carried out on the interactions of geopolymers with pesticides in water, no research work has reported the use of municipal waste incineration fly ash (MWFA)-based geopolymers as adsorbents for endosulfan removal from contaminated water. MWFA-based geopolymers are of great interest in pesticide remediation due to the dual advantage of valorization of waste materials and water treatment with the possibility of using the spent geopolymers for construction purposes (Tome et al., 2018).

During geopolymer formation, an aluminosilicate source with sufficient aluminum and silicon percentage composition is allowed to react with an alkaline activator solution (Siyal et al., 2018). The type of aluminosilicate source, the concentration and type of the alkaline activator solution, and the curing temperature affect the properties of the geopolymer formed (Tome et al., 2018; Tome et al., 2021). The disposal of MWFA is an unresolved environmental problem that causes secondary pollution. Since MWFA is reported to have sufficient aluminum and silicon content, it can be applied as an aluminosilicate precursor during geopolymer formation (Fabricius et al., 2020). Al-Ghouti et al. (2020) reported the use of MWFA-based geopolymers for the removal of dyes from water. However, the effect of synthesis conditions for optimization of the adsorption properties of MWFA-based geopolymers has not been reported as well. This leaves a gap in our understanding of the optimum conditions for maximization of the adsorptive potential of MWFA-based geopolymers. In this study, the precursor material (MWFA) is reacted with alkaline activator solutions of varied sodium silicate to sodium hydroxide (SS/SH) ratios to obtain various morphologically different MWFA-based geopolymers. The effect of the SS/SH ratios on the textural and adsorption properties of the MWFA-based geopolymers was

investigated, with endosulfan introduced in water as a model pesticide and is herein reported.

2 Materials and methods

2.1 Materials and reagents

The municipal waste fly ash (MWFA) was collected from Environmental Combustions and Consultancy Limited, Migori, Kenya. An amount of 90 g of MWFA was crushed, sieved using a 100-µm pore size sieve, and stored in a vacuum desiccator. Analytical reagent (AR) grade sodium hydroxide (NaOH), sodium silicate ($Na_2SiO_3.9H_2O$), endosulfan (6,9-methano-2,4,3-benzodioxathiepin,6,7,8,9,10,10-hexachloro-1,5,5a,6,9,9a-hexahydro-3,3-dioxide), hydrochloric acid (HCl), and sodium chloride (NaCl) were purchased from Kobian Scientific Limited, Kenya.

2.2 Methodology

2.2.1 Synthesis of the geopolymer adsorbents

For the synthesis, 50 mL solution of 8 M NaOH was prepared in a polypropylene beaker using a magnetic stirrer. Then, the solutions were covered and left to cool to room temperature. Then, three 15 mL portions of the 8 M NaOH solution were transferred into three different polypropylene beakers labeled A, B, and C, and to them, 5.81, 6.98, and 8.14 g of sodium silicate (SS) were added, respectively. The activator solutions were stirred at 800 rpm and at a temperature of 40°C for 30 min to obtain homogeneous mixtures. The activator solutions were kept covered with a parafilm to prevent carbonation and allow for complete de-polymerization of sodium silicate for 24 h.

Activator solutions were mixed with the municipal waste fly ash (MWFA) at a solid-to-liquid (S/L) ratio of 2 and shaken for 5 min at 150 rpm to form pastes. The fly ash-based geopolymer pastes were transferred into cylindrical containers and then cured at 25°C for 24 h. The three cured geopolymers, that is, MWFA-based geopolymer A (GPA), MWFA-based geopolymer B (GPB), and MWFA-based geopolymer C (GPC), were then crushed and sieved to pass a 100-µm sieve, and stored in a desiccator before use.

2.3 Characterization of the geopolymer adsorbents

Morphology, microstructure, and percentage elemental composition of the geopolymers and MWFA were obtained by scanning electron microscopy–energy dispersive spectroscopy, SEM-EDS (JSM-IT500). Sample crystallinity was acquired using a Bruker D8 Advance X-ray diffractometer with copper Kα wavelength, Kα = 1.5406 Å. Functional groups of the MWFA-based geopolymers and MWFA were examined using an FTIR spectrophotometer (NICOLET iS50 FT-IR) at 400–4000 cm^{-1} wavenumbers. The point of zero charge is the pH at which the net charge on the adsorbent surface is zero. The pH point of the zero charge of MWFA and the synthesized geopolymers (pH_{pzc}) was determined using the pH drift method (Dzoujo et al., 2022; Hermann et al., 2022).

2.4 Batch adsorption experiments

The initial endosulfan concentrations used in the adsorption experiments were 0, 4, 8, 12, 16, and 20 mg/L. Contact time, pH, temperature, and adsorbent dosage were kept constant at 90 min, 5,303 K, and 0.1 g/50 mL endosulfan solution, respectively. The mixtures were filtered after equilibration, and the residual endosulfan concentration in the filtrate was determined spectrophotometrically at $\lambda_{max} = 212\ nm$.

The amount of endosulfan adsorbed at equilibrium, mg/g, was calculated as

$$q_e = \frac{(C_i - C_e)V}{M}, \tag{1}$$

where C_i and C_e are the initial and equilibrium endosulfan concentrations (mg/L), respectively. V is the volume, L, of the solution, and m is the mass, g, of the adsorbent.

The amount of endosulfan adsorbed (q_t) onto the geopolymers at any given time, (t), was given by

$$q_t = \frac{(C_i - C_t)V}{M}, \tag{2}$$

where C_t is the adsorbate concentration (mg/L) at any given time. Adsorption removal efficiency (η) at equilibrium time was calculated as

$$\eta = \left[\frac{C_i - C_f}{C_i}\right] \times 100, \tag{3}$$

where C_i and C_f were the initial and final concentrations, respectively.

Additionally, the effect of pH was investigated in the pH range of 2.0–10.0. The adsorbent dosage, contact time, initial endosulfan concentration, and temperature were kept constant at 0.1 g/50 mL solution, 90 min, 8 mg/L, and 303 K, respectively. Then, 0.1 M HCl and 0.1 M NaOH were used to adjust the pH of the solution accordingly.

The effect of contact time was studied at predetermined intervals of 0, 10, 20, 30, 40, 50, 60, 90, 120, and 150 min. The adsorbent dosage, pH, initial endosulfan concentration, and temperature were kept constant at 0.1 g/50 mL solution, 5, 8 mg/L, and 303 K, respectively. An aliquot of the supernatant was then extracted to determine residual endosulfan.

To investigate the effects of temperature, the adsorption processes were studied to establish its thermodynamic characteristics in the temperature range of 303–353 K in a temperature-controlled shaker at 150 rpm (Shaking Incubator, Model: SSI10R-2, Orbital-Shaking) for a stipulated fixed duration. The contact time, pH, initial endosulfan concentration, and geopolymer dosage were kept constant at 90 min, 5, 8 mg/L, and 0.1 g/50 mL solution, respectively.

Adsorbent dosage was also investigated when different amounts of the adsorbent, from 0.05 to 0.3 g, were used in 50 mL of the endosulfan solution. The contact time, pH, initial endosulfan

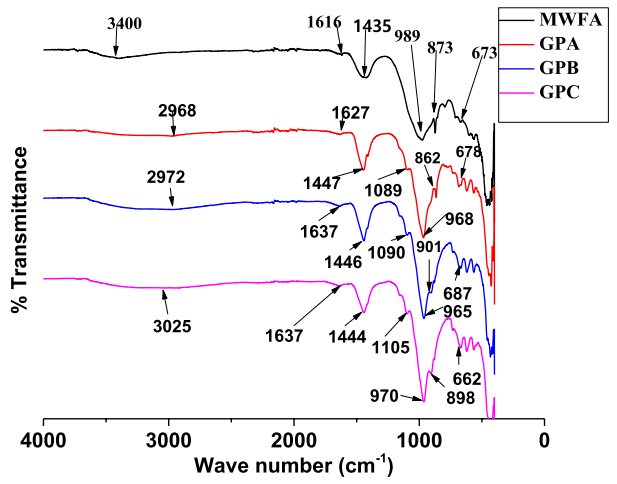

FIGURE 1
FTIR spectra of MWFA and MWFA-based geopolymers GPA, GPB, and GPC.

concentration, and temperature were kept constant at 90 min, 5, 8 mg/L, and 303 K, respectively.

2.5 Data analysis

The statistical difference was tested using one-way analysis of variance, and data were presented using linear regression in graphical format by OriginPro 9.0 software.

3 Results and discussion

3.1 Characterization studies

3.1.1 Functional group identification

FTIR plots (Figure 1) present the functional groups present in MWFA and MWFA-based geopolymers. For MWFA, there are strong absorption bands at 3,400 and 1,435 cm^{-1}, and a pre-eminent band at 989 cm^{-1}. Other important bands are centered between 400 and 800 cm^{-1} wavenumbers.

A comparison of MWFA-based geopolymers with MWFA shows some changes in the bands. The presence of quartz in MWFA avails Si-O-T (T-tetrahedral Al or Si) bonds responsible for the band at 989 cm^{-1} (Siyal et al., 2019). The shift in this band to lower wavenumbers (968, 965, and 970 cm^{-1}) in the MWFA-based geopolymers GPA, GPB, and GPC shows that some quantity of metasilicate participated in the geopolymerization reaction.

The bands at 989 and 673 cm^{-1} correspond to the asymmetric and symmetric stretch vibrations of aluminosilicate tetrahedral, Si-O-T (T-tetrahedral Al or Si) bonds in MWFA. The asymmetric stretch vibration bands reduced to lower wavenumbers (968, 965, and 970 cm^{-1}), increased in intensity, and narrowed with the synthesis of GPA, GPB, and GPC, respectively. According to Daud et al. (2021), Si-O-T gives the main band used as evidence of geopolymer synthesis. During geopolymerization, there is bond breaking and bond formation is responsible for the variations in the main band (Siyal et al., 2016). The shift in these main bands to lower wavenumbers was evidence that changes occurred in the angle and length of the Si-O-Si bonds, indicating that the SS/SH ratios contribute significantly to the structure of the prepared geopolymers (Innocenzi et al., 2003).

The bands at 3,400 and 1,616 in MWFA are due to stretching and deformation vibrations of H-O-H and -OH bonds (Zhang et al., 2012). The stretching vibrations of H-O-H and –OH bands appear at 2,968, 2,972, and 3,025 cm^{-1} for GPA, GPB, and GPC, respectively. The deformation vibrations of –OH bands appear at 1,627, 1,637, and 1,637 cm^{-1} for GPA, GPB, and GPC, respectively. The H-O-H and -OH bond bands indicate the presence of water and silanol groups (Tome et al., 2018). The silanol group and water molecules trapped in the geopolymer hollows are responsible for the shifts in the deformation vibrations of –OH bands to higher wavenumbers (Zhang et al., 2012; Liu et al., 2016). Previous related geopolymer studies also reported similar trends in FTIR analysis, confirming the successful synthesis of geopolymers GPA, GPB, and GPC (Nath and Sarker, 2017; Sarkar et al., 2017).

3.1.2 Morphological and composition analyses

The morphological and structural analyses of MWFA, GPA, GPB, and GPC obtained from SEM-EDX images are shown in Figure 2. MWFA appears to have different morphological features and agrees with the findings of El Alouani et al. (2018), which reported loosely packed structures with high porosity. One clear observation is the uniform granular, tiny, spherical, and loosely packed structures in the geopolymers, which provides evidence that geopolymerization occurred (El Alouani et al., 2018; Maleki et al., 2019). The absence of tiny spherical structures in GPA, GPB, and GPC indicates almost complete geopolymerization of the precursor materials into crystalline geopolymers. Comparatively, the spongy and gel-like morphology is more elaborate in GPC and GPB than in GPA (Al-Ghouti et al., 2020). The presence of pores and cavities on the surfaces of the adsorbents is the key factor for endosulfan removal from wastewater by adsorption (Shokrollahi et al., 2011; Ghani et al., 2020).

The percentage elemental composition of MWFA and the prepared geopolymers are shown in Table 1. The Si/Al ratios in MWFA and the geopolymers were found to be different. The changes in elemental composition arose from the alkaline activator solutions used. The MWFA-based geopolymers had Si/Al ratios lower than 2.4, indicating that they had polysialate-siloxo (-Si-O-Al-O-Si-O-) structure (El Alouani et al., 2018). The amount of heavy metals in MWFA and the MWFA-based geopolymers was undetectable, indicating the unlikely possibility of secondary pollution from the adsorbents (Ghani et al., 2020).

3.1.3 Crystallinity and mineralogical studies

The diffractograms of the three studied geopolymers GPA, GPB, and GPC, and the aluminosilicate source (MWFA) used for the synthesis are shown in Figure 3. Sharp peaks indicate a crystalline phase, while a hump shows the presence of an amorphous phase. The crystalline phases, degree of crystallinity (DOC), and amorphous contents were determined using the Rietveld method on Match XRD software. The DOC is calculated by dividing the total

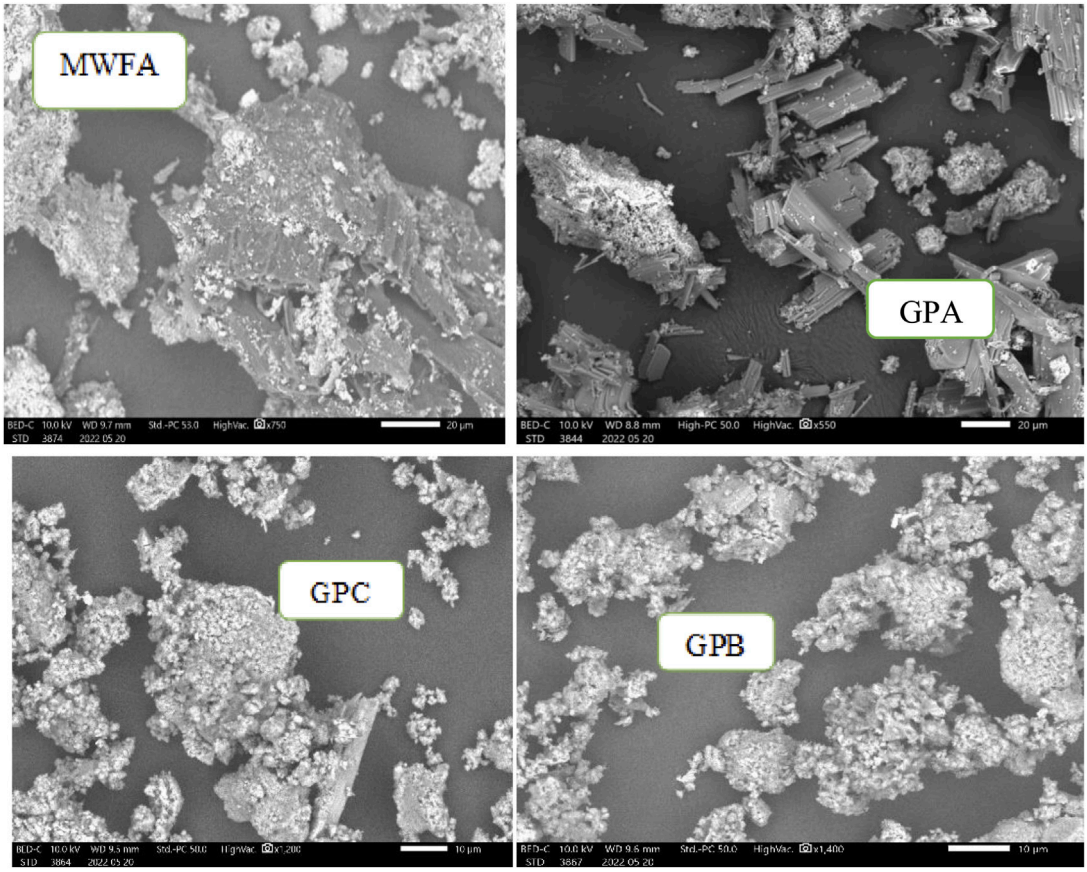

FIGURE 2
SEM images of MWFA (×750), GPA (×550), GPB (×850), and GPC (×1,200).

TABLE 1 EDX elemental composition.

	Element	O	Mg	Na	Al	Si	Ca	Si/Al
MWFA	% Mass	56.84	2.26	-	8.34	9.84	23.08	1.18
GPA	% Mass	61.83	-	25.78	3.36	6.41	2.62	1.91
GPB	% Mass	55.29	-	19.40	8.65	16.66	-	1.93
GPC	% Mass	53.86	-	22.76	7.77	15.61	-	2.01

area of the crystalline peaks by the total area under the diffraction curve. On the other hand, the amorphous content is calculated by dividing the total area of amorphous peaks by the total area under the diffraction curve. The raw data on the diffraction patterns were analyzed using Match XRD software. For a selected phase, the total area of matched peaks divided by the total area of the crystalline phase peaks gives the phase quantification.

MWFA had a DOC of 17.40%, and the amorphous content was 82.60% by weight. The following four crystalline phases were identified in MWFA: 37.3% grossular ($Al_2Ca_3O_{12}Si_3$) (cubic crystal system) [PDF# 96-900-0442], 34.4% cristobalite (SiO_2) (tetragonal) [PDF# 96-900-1581], 21.2% quartz (SiO_2) (trigonal–hexagonal axes) [PDF# 96-901-1495], and 7.2% kalsilite ($AlKO_4Si$) (hexagonal) [PDF# 96-900-9729]. The unidentified peak area was 13.3%.

The GPA had a DOC of 20.45%, and the amorphous content was 79.55% by weight. The following four crystalline phases were identified in GPA: 47.3% lisetite ($Al_{3.96}Ca_{0.98}Na_{1.97}O_{16}Si_{4.04}$) (orthorhombic) [PDF# 96-900-1030], 23.2% albite ($AlNaO_8Si_3$) [triclinic (anorthic)], [PDF# 96-900-3701], 19.3% jadeite ($AlNaO_6Si_2$) (monoclinic) [PDF# 96-900-0344], and 10.1% barroisite ($Al_2CaH_2Mg_3NaO_{24}Si_8$) (monoclinic) [PDF# 96-901-6521]. The unidentified peak area was 15.0%.

The GPB had a DOC of 14.88%, and the amorphous content was 85.12% by weight. The following three crystalline phases were identified in GPB: 52.4% kumdykolite ($AlNaO_8Si_3$) (orthorhombic), [PDF# 96-154-4371], 25.1% melilite ($AlCaNaO_7Si_2$) (tetragonal), [96-900-8196], and 22.5% albite ($AlNaO_8Si_3$) (triclinic (anorthic)), [PDF# 96-900-3702]. The unidentified peak area was 11.4%.

The GPC had a DOC of 21.26%, and the amorphous content was 78.74% by weight. The following two crystalline phases were identified in GPC: 53.2% albite ($AlNaO_8Si_3$) (triclinic (anorthic)), [PDF# 96-900-0586] and 46.8% lisetite ($Al_{3.96}Ca_{0.98}Na_{1.97}O_{16}Si_{4.04}$) (orthorhombic), [PDF# 96-900-1030]. The unidentified peak area was 17.4%. The changes in SS/SH ratios favored the formation of

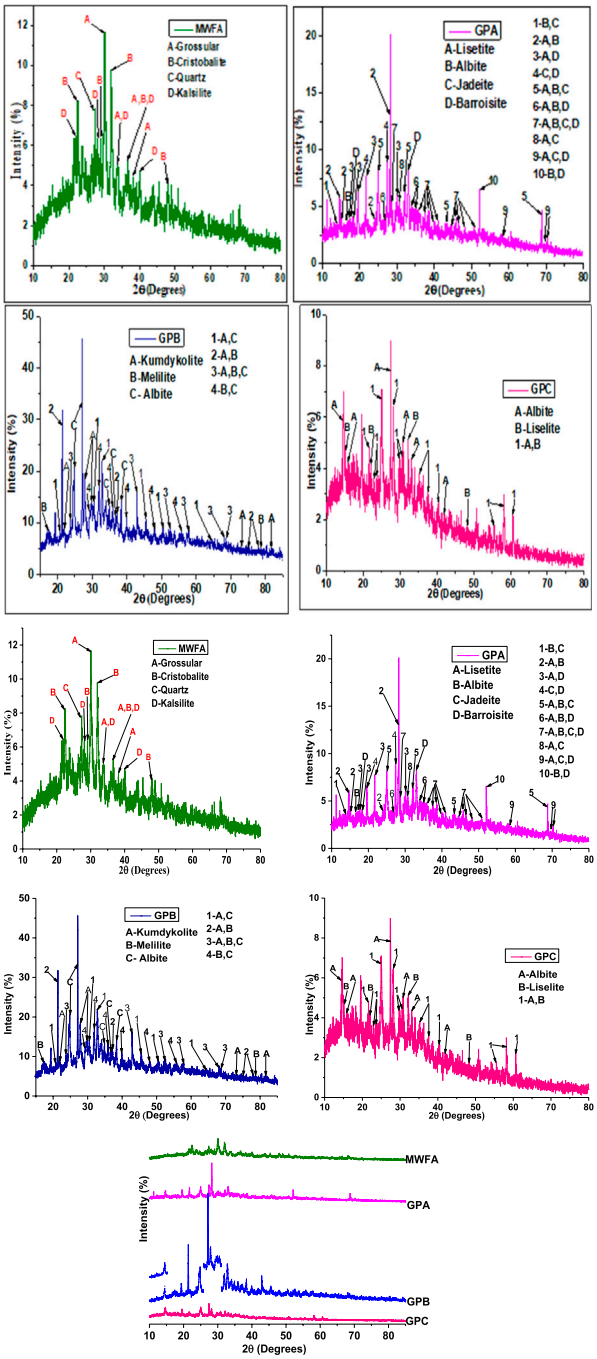

FIGURE 3
XRD spectra for MWFA, GPA, GPB, and GPC.

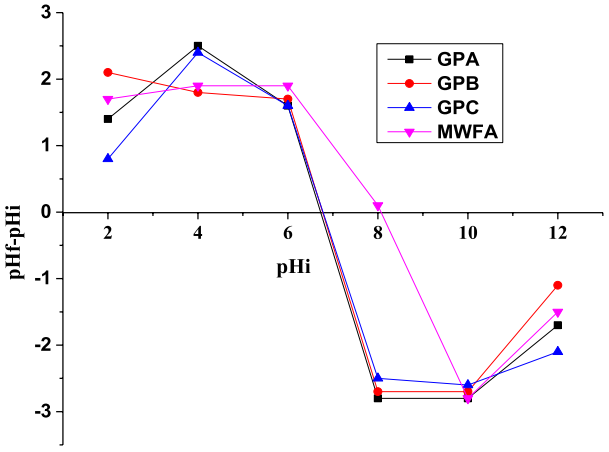

FIGURE 4
pH point of zero charge of MWFA, GPA, GPB, and GPC.

new mineral phases, resulting in geopolymers with varied chemical compositions (El Alouani et al., 2018).

3.1.4 Point of zero charge (pH_{pzc}) studies

Designing adsorption-based separation techniques between a solid and liquid phase depend on the surface chemistry of the adsorbent described by its point of zero charge (pH_{pzc}). pH_{pzc} is the average pH value of the adsorbent in the NaCl electrolyte. pH_{pzc} was found to be at pH 8.1, 6.8, 6.7, and 6.8 for MWFA, GPA, GPB, and GPC, respectively (Figure 4). For instance, GPB becomes positively charged below pH 6.7, neutral at pH 6.7, and negatively charged above pH 6.7. pH_{pzc} is observed to be independent of the SS/SH ratios of the alkaline activator solution. Values comparable to those in this study and similar findings have been reported by Sarkar et al. (2019) and Hermann et al. (2022).

3.2 Adsorption experiments

3.2.1 Effect of pH and the adsorption mechanism

There was a decrease in geopolymer adsorption capacities as the pH increased (Figure 5) (Zió lkowska et al., 2009). At lower pH conditions (below pHpzc 6.8), the Si and Al centers of the geopolymer and water molecules become protonated due to a high concentration of H^+ ions. As a result, the adsorbent surface becomes positively charged (GP^+) and the negatively charged endosulfan moieties (pKa = −5.5) are electrostatically attracted to the geopolymer surface (Rauf et al., 2012; Kakoi et al., 2015). At higher pH, the Si-OH and Al-OH bonds of the geopolymer become deprotonated to acquire a negative charge. Consequently, Coulombic repulsion forces between the adsorbent surface and adsorbate molecules become significant, resulting in decreased adsorption. The decrease in adsorption at high pH is also attributed to competition between the hydroxide ions (OH^-) and negatively charged endosulfan for the same adsorption sites. Very low pH ranges are unsuitable for practical application. The optimum pH was found to be 5.0, as shown in Figure 5. In addition to electrostatic interactions, hydrogen bonding between hydrogen in the hydroxyl (–OH) groups on the adsorbent surface and the lone pairs of electrons of the electronegative O and Cl atoms of endosulfan is proposed.

3.2.2 Effect of the initial concentration

The adsorption capacity was found to increase with an increase in the initial concentration (Figure 6). At low concentrations, the majority of the adsorption sites remained unoccupied due to low adsorbate/adsorbent interactions. An increase in the initial

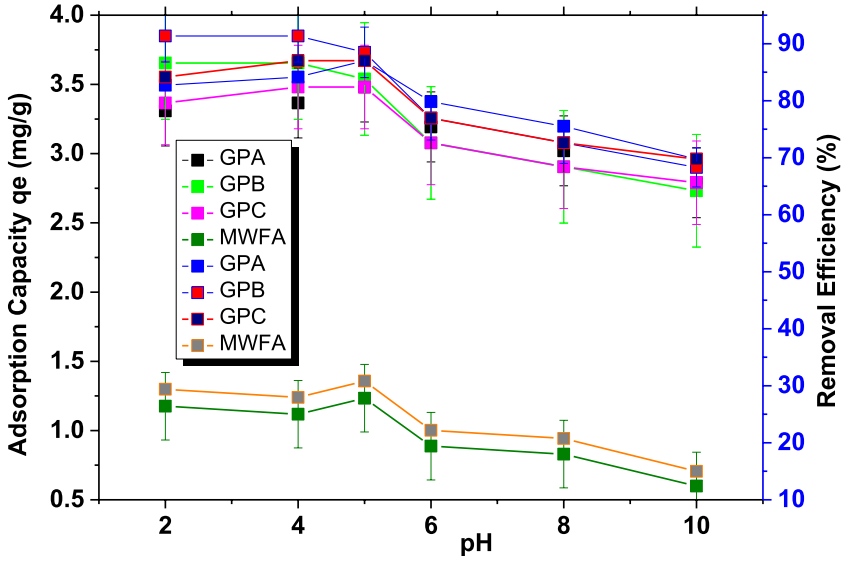

FIGURE 5
Graph of pH against the adsorption capacity and removal efficiency.

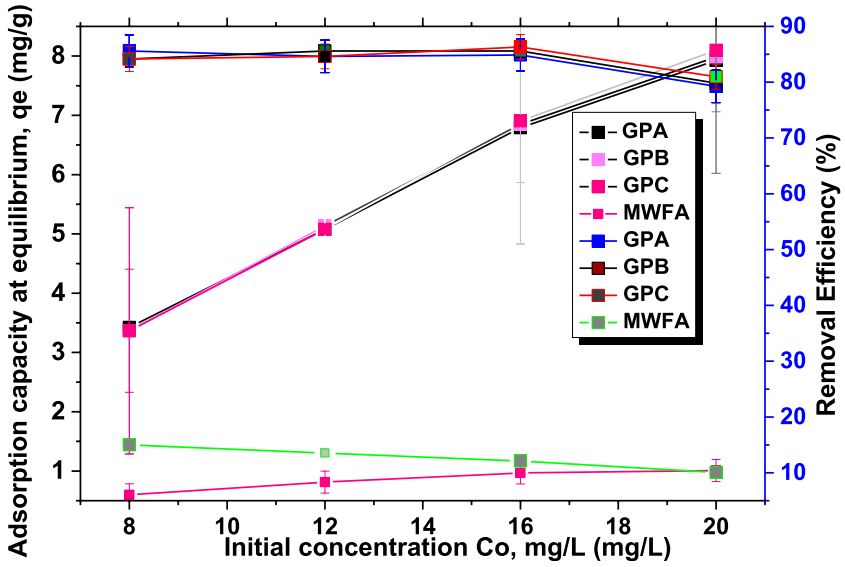

FIGURE 6
Effect of the initial concentration on the adsorption capacity and removal efficiency.

concentration led to increased adsorbate/adsorbent interactions and mass gradient between the solid phase and the bulk solution until the maximum adsorption capacity was reached (Maingi et al., 2017).

3.2.3 Effect of contact time

The time-dependent evolution of the geopolymer sorption capacity for endosulfan depicted fast sorption kinetics, leading to saturation within 90 min (Figure 7), followed by an equilibrium phase. It is worth noting that the geopolymers exhibited higher removal efficiencies for endosulfan (>83%) than MWFA (20.58%). Geopolymerization improved the removal efficiency of the raw material by approximately four orders of magnitude (Gupta et al., 2021).

3.2.4 Kinetics studies

The adsorption kinetics for endosulfan onto geopolymers were analyzed using linearized Lagergren *pseudo*-first-order (PFO) (Eq. 4) (Yuh-Shan, 2004) and *pseudo*-second-order (PSO) (Eq. 7) (Ho and McKay, 1999; Revellame et al., 2020) kinetic models.

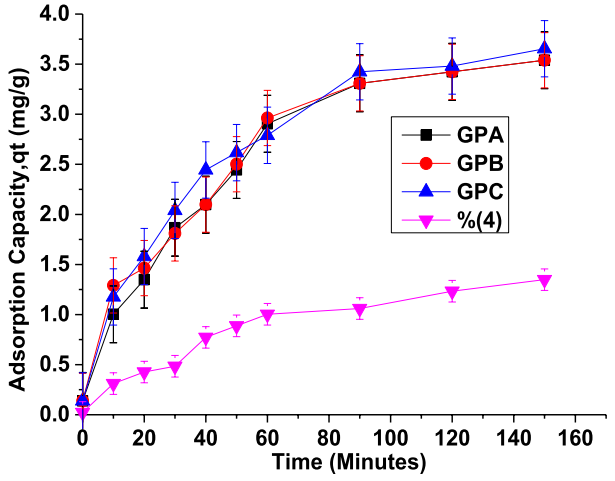

FIGURE 7
Evolution of the sorption capacity of MWFA-based geopolymers (GPA, GPB, GPC, and MWFA) for endosulfan with time (m = 0.1 g/50 mL, C_i = 8 mg/L, and pH = 5).

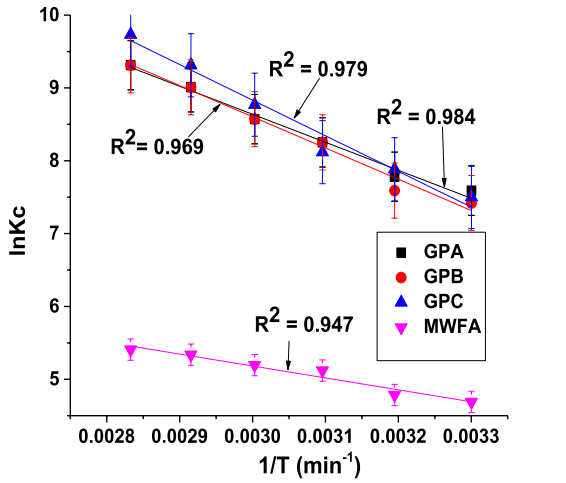

FIGURE 8
Van't Hoff plots.

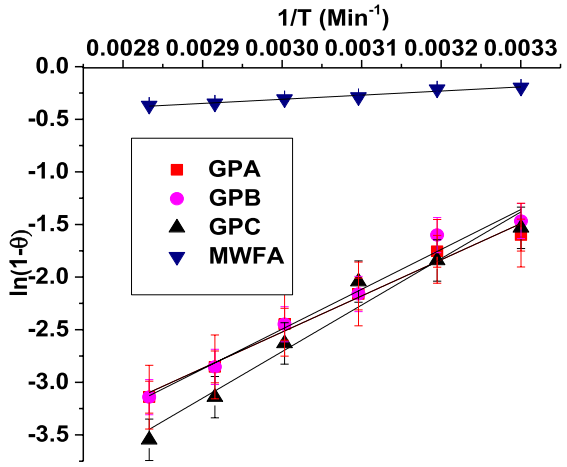

FIGURE 9
Arrhenius-type equation plots.

TABLE 2 Lagergren *pseudo*-first-order (PFO) and *pseudo*-second-order (PSO) data.

Model	Parameter	GPA	GPB	GPC	MWFA
PFO	K_1 (min^{-1})	0.024	0.026	0.028	0.019
	q_e (cal) (mg g^{-1})	3.661	3.604	3.635	1.399
	q_e (exp) (mg g^{1})	3.308	3.308	3.424	1.061
	S rate ($mg.g^{1}.min^{-1}$)	0.088	0.093	0.102	0.027
	$t_{\frac{1}{2}}$ (min)	28.88	26.66	24.76	36.48
	R^2	0.978	0.974	0.996	0.955
PSO	K_2 (g mg^{1} min^{1})	0.027	0.027	0.028	0.009
	q_e (cal) (mg g^{-1})	0.689	0.690	0.691	0.688
	q_e (exp) (mg g^{1})	3.308	3.308	3.424	1.061
	S rate ($mg.g^{1}.min^{-1}$)	0.128	0.129	0.134	0.004
	$t_{\frac{1}{2}}$ (min)	53.75	53.68	51.68	161.5
	R^2	0.875	0.880	0.895	0.847

$$q_t = q_e\left(1 - e^{-k_1 t}\right), \tag{4}$$

where k_1 is the PFO rate constant (min^{-1}), q_e (mg/g) is the adsorption capacity at equilibrium, and q_t (mg/g) is the adsorbed amount of adsorbate at any given time (minutes). Assuming PFO kinetics, the initial adsorption rate and adsorption half-life were calculated using Eqs 5, 6, respectively.

$$S_{rate} = k_1 q_e, \tag{5}$$

$$t_{\frac{1}{2}} = \frac{\ln 2}{k_1}. \tag{6}$$

The pseudo-second-order kinetic model is given as

$$q_t = \frac{q_e^2 k_2 t}{1 + k_2 q_e t}, \tag{7}$$

where k_2 is the PSO rate constant (g/mg/min).

The initial sorption rate (S_{rate}) and the adsorption half-life ($t_{1/2}$) for PSO were obtained from Eqs 8, 9, respectively, (Ho and McKay, 1999). The computed values are presented in Table 2:

$$S_{rate} = k_2 q_e^2, \tag{8}$$

$$t_{\frac{1}{2}} = \frac{1}{k_2 q_e}. \tag{9}$$

From Table 2, since the coefficients of determination (R^2) values for the PFO were closest to unity than PSO, the adsorption kinetics were best accounted for and predicted by the PFO kinetic model. The plots are in the supplementary document. The initial adsorption rates (S_{rate}) decreased in the order 0.102 > 0.093 > 0.088 > 0.027 for GPC, GPB, GPA, and MWFA, respectively, with a decrease in SS/SH ratios. The rate constant (k_1) showed minute

TABLE 3 Obtained thermodynamic parameters of GPA, GPB, GPC, and MWFA.

	GPA			GPB			GPC			MWFA		
T (K)	ΔH	ΔG	ΔS	ΔH	ΔG	ΔS	ΔH	ΔG	ΔS	ΔH	ΔG	ΔS
303	31.98	−19.12	167.75	35.65	−18.69	178.48	40.67	−18.90	195.44	13.61	−11.81	83.91
313		−20.26			−19.75			−20.52			−12.45	
323		−22.16			−22.16			−21.80			−13.75	
333		−23.73			−23.73			−24.28			−14.38	
343		−25.69			−25.69			−26.55			−15.22	
353		−27.33			−27.33			−28.56			−15.87	

variation across the geopolymer adsorbents. The adsorption rate (k_1) was, therefore, weakly influenced by the chemical composition of the materials (El Alouani et al., 2018; Gupta et al., 2021). At the onset, when all adsorption sites are vacant, the GPC had the highest initial adsorption rate (S_{rate}), indicating that it had the highest number of energetically favorable and accessible adsorption sites, thus controlling the adsorption half-life ($t_{1/2}$). The SS/SH ratios of the activator solution had a bearing on the accessibility of the favored adsorption sites. Conformity to PFO suggests a physisorption-mediated rate-determining step (El Alouani et al., 2018; Revellame et al., 2020; Gupta et al., 2021).

3.2.5 Effect of temperature on adsorption of endosulfan

Temperature rise led to an increase in the amount of endosulfan adsorbed, indicating an endothermic reaction. As the temperature increased, the kinetic energy of endosulfan molecules increased, increasing the number of interactions with active sites. An increase in temperature also decreased the boundary layer, and this led to an increase in adsorption.

3.2.6 Thermodynamics

The effect of temperature changes on the sorption was studied in the range 303–353 K. The thermodynamic parameters, namely, change in Gibb's free energy (ΔG), enthalpy (ΔH), and entropy (ΔS), which indicate the practical feasibility of the process, post-adsorption structural changes of the adsorbent, and the adsorption mechanism, were derived from the Van't Hoff Eq. 13 (Figure 8).

$$\Delta G = -RT \ln K_c, \tag{10}$$

$$K_c = 1000 K_d, \tag{11}$$

$$K_d = \frac{C_{ads}}{C_e}, \tag{12}$$

$$\ln K_c = \frac{\Delta S}{R} - \frac{\Delta H}{RT}, \tag{13}$$

where K_c is the dimensionless equilibrium constant, T is the temperature (Kelvin), and R is the universal gas constant (8.314 J/mol. K). C_e is the equilibrium endosulfan concentration in the solution (mg/L), and C_{ads} represents the equilibrium endosulfan concentration in the solid phase (mg/g). K_d is the distribution coefficient (L/g), and the density of water is 1,000 g/L (Hermann et al., 2022).

The positive ΔH values for all the geopolymers indicated an endothermic process. All the enthalpy values were very low (≤40 kJ/mol), which corresponds to physisorption processes (Jemutai-Kimosop et al., 2022).

The positive ΔS value indicated that, at the liquid–solid interface, there was an increased disorderliness and an affinity of the adsorbent for the adsorbate (Shikuku et al., 2018a).

The negative ΔG values (Table 3) indicated that the adsorption processes were spontaneous and favorable. The relatively low magnitudes of ΔG values support the aforementioned physical adsorption mechanism (Dzoujo et al., 2022; Hermann et al., 2022). The thermodynamics data show that the adsorption of endosulfan by the geopolymers is an entropy-driven process.

The sticking probability, S*, and adsorption activation energy (E_a) were computed from experimental data using the modified Arrhenius-type equation (Eq. 14) related to surface coverage (θ) by the relation (Shikuku et al., 2018a):

$$\ln(1-\theta) = \ln S^* + \frac{E_a}{R}\frac{1}{T}. \tag{14}$$

The value of θ was determined using the following equation:

$$\theta = \left[1 - \frac{C_e}{C_i}\right]. \tag{15}$$

The activation energies (in kJ/mol) for the adsorption processes were found to be 28.57, 31.49, 36.78, and 3.25 for GPA, GPB, GPC, and MWFA, respectively (Figure 9). The E_a values and ΔH values are all lower than 40 kJ/mol, and this consistency confirmed physical adsorption processes.

S* depends on the adsorbate/adsorbent system under study and temperature. The S* value lies in the range $0 < S^* < 1$. The S* values were found to be 2.6676×10^{-6}, 9.5622×10^{-7}, 1.1482×10^{-7}, and 2.2630×10^{-1} for GPA, GPB, GPC, and MWFA, respectively. The sticking probability (S*) was found to be very low, indicating a low probability for the endosulfan molecules to stick on the adsorbent surface upon collision, a testament to a physisorption mechanism with no exchange of electrons (Shikuku et al., 2018a).

3.2.7 Adsorption isotherms

Eq. 16 describes the Langmuir isotherm (Langmuir, 1918):

TABLE 4 Langmuir and Freundlich isotherm model data.

	Langmuir isotherm model					Freundlich isotherm model				
	Q_O	K_L	Ka	R_L	R^2	R^2	K_F	q_m	1/n	n
GPA	15.899	0.258	4.10	0.162	0.971	0.943	3.288	23.676	0.659	1.517
GPB	16.970	0.238	4.04	0.174	0.951	0.921	3.301	25.162	0.678	1.475
GPC	20.010	0.191	3.82	0.207	0.944	0.923	3.229	28.848	0.731	1.368
MWFA	1.872	0.070	0.13	0.417	0.987	0.964	0.184	1.141	0.609	1.642

$$q_e = \frac{Q_0 K_L C_e}{1 + K_L C_e}. \quad (16)$$

Ce represents the equilibrium concentration of the endosulfan adsorbate (mg/L), while q_e is the amount of endosulfan adsorbed at equilibrium (mg/g). Q_o represents the monolayer maximum adsorption capacity (mg/g), and the Langmuir adsorption constant, K_L (L/mg), is related to the free energy of adsorption.

According to the Langmuir isotherm model, there occurs single-layer adsorption of adsorbate molecules onto a fixed number of active sites and there was no lateral interaction between adsorbed molecules on a morphologically homogeneous surface. The adsorption sites are, in this case, considered to be identical (Peydayesh et al., 2015; Karaer and Kaya, 2016; Karaer and Kaya, 2016; Zulkifly et al., 2019).

Eq. 17 describes the Freundlich isotherm expressed using a dimensionless parameter called the separation factor (R_L), as follows:

$$R_L = \frac{1}{1 + K_L C_i}. \quad (17)$$

The following equation expresses the Freundlich isotherm:

$$q_e = K_F C_e^{1/n}, \quad (18)$$

where q_e (mg/g) is the adsorbed amount of adsorbate at equilibrium. Freundlich constant, K_F, ((mg/g) × (L/mg)$^{1/n}$)) indicates the relative adsorption capacity of the adsorbent (mg/g); "n" is the Freundlich exponent, and 1/n is the Freundlich intensity parameter, a constant that shows the intensity of the adsorption. The C_e (mg/L) value was the equilibrium concentration of the adsorbate.

The Freundlich equation has two constants K_F and 1/n for a given adsorbent and adsorbate, respectively, at a particular temperature. The high K_F and low values of 1/n indicate high adsorption throughout the concentration range studied; whereas high values of 1/n and low K_F values indicate low adsorption (Treybal, 1980). The Freundlich intensity parameter also shows surface heterogeneity, where it becomes more heterogeneous as its value gets closer to zero.

The Freundlich equation is exponential; therefore, the amount of adsorbate on the adsorbent surfaces rises with an increase in the solute concentration. Using Eq. 19, Halsey determined the assumed Freundlich maximum adsorption capacity (Halsey, 1948):

$$q_m = K_F C_i^{1/n}, \quad (19)$$

where C_i is the initial solute concentration (mg/L) and q_m is the Freundlich maximum adsorption capacity (mg/g).

TABLE 5 Comparison of adsorption capacities of MWFA-based geopolymers with other adsorbents for endosulfan.

Adsorbent	Q_o (mg/g)	Reference
Wood charcoal	0.530	Yedla and Dikshit (2008)
Amine-modified magnetic diatomite	97.200	Alacabey (2022)
Raw diatomite	16.600	Alacabey (2022)
Carbon slurry	34.110	Gupta and Imran (2008)
Activated charcoal	2.145	Sudhakar and Dikshit (1999)
Wood charcoal	1.773	Sudhakar and Dikshit (1999)
Sojar caju	1.575	Sudhakar and Dikshit (1999)
Kimberlite tailings	0.882	Sudhakar and Dikshit (1999)
Silica	0.323	Sudhakar and Dikshit (1999)
GPA	15.899	This study
GPB	16.970	This study
GPC	20.010	This study
MWFA	1.872	This study

The equilibrium data were tested against the two classical non-linear adsorption models. The non-linear regression was performed by minimization of the values of the regression sum of squares (RSS) expressed as Shikuku et al. (2018b)

$$\mathrm{RSS} = \sum_{1}^{N} \left(q_{e,experimental} - q_{e,predicted}\right)^2. \quad (20)$$

The best-fitting model was determined using the coefficient of determination (R^2) values. The relatively high coefficient of determination (R^2) values (Table 4) indicate that the adsorption of endosulfan onto the geopolymers was best predicted by the Langmuir isotherm. The R_L values were between 0 and 1 for all the adsorbents, indicating that the adsorption processes are favorable (Meroufel et al., 2013).

The monolayer maximum adsorption capacities (Q_o) are 15.89, 16.97, 20.01, and 1.87 mg/g for GPA, GPB, GPC, and MWFA, respectively. It is worth noting that the adsorption capacities of the geopolymers were substantially higher (~8–10 times) than that of

MWFA, attesting that geopolymerization was a beneficial step. Additionally, the adsorption capacity of the geopolymers increased with increasing SS/SH ratios. The apparent equilibrium constant (Ka), a product of Q_{max} and K_L, derived from the Langmuir isotherm, is a measure of the relative affinity of the adsorbent toward the endosulfan molecules (Mishra and Tiwari, 2006). The apparent equilibrium constant values (Table 4) indicate that the affinity of the geopolymers for endosulfan is much higher (~30 times) than that of MWFA. Additionally, the geopolymers had a similar affinity toward endosulfan. This shows that the difference in chemical compositions of the geopolymers, from the XRD data, could not account for the trends in their adsorption capacities. This is further supported by the FTIR data that showed no new functional groups that would induce increased affinity. The increase in adsorption capacity with an increase in SS/SH ratios is attributed to increased accessibility to the energetically favored binding sites. The adsorption capacity of geopolymers is, therefore, neither necessarily nor solely controlled by their composition. A trade-off between composition and textural properties is inferred.

On the other hand, the Freundlich model (Freundlich, 1906) proposes multilayer adsorption. This kind of adsorption has differing dispersion of adsorption affinities onto the heterogeneous surface of the adsorbent without any lateral interaction. In line with this postulate, the adsorption sites which are energetically favored are occupied first, followed by those having diminishing binding energies with increasing rates of site occupancy.

KF and 1/n for the geopolymers were higher than MWFA, indicating that geopolymerization improved the affinity for endosulfan. However, the KF values for the geopolymers were invariable (Table 4), indicating that the affinity of the geopolymers for endosulfan was independent of the composition. This is consistent with the apparent equilibrium constants (Ka) from the Langmuir isotherm. The Freundlich factor (1/n) values less than unity correspond to heterogeneous adsorbent surfaces. Additionally, the magnitudes of 1/n suggest weak adsorbent–adsorbate interactions corresponding to the physisorption mechanism (Shikuku and Kimosop, 2020). This is supported by the thermodynamics data.

The adsorption capacities of the geopolymers in this study were compared to those of adsorbents reported in the literature for the removal of endosulfan from water (Table 5). It is observed that the adsorption capacity of geopolymers, especially GPC, was higher than that of most of the adsorbents. MWFA-based geopolymers are, therefore, promising adsorbents for the sequestration of endosulfan from water.

Conclusion

A total of three MWFA-based geopolymers GPA, GPB, and GPC were synthesized *via* alkaline activation with increasing SS/SH ratios, and the products were used to adsorb endosulfan from water. SEM/EDS detected a highly inhomogeneous glass-like matrix, constituted mainly of Na-Si-Al phases in a bulk region, together with unreacted spheres of MWFA particles. The geopolymerization reaction is evidenced by the shift in the Si–O–T (T = Si or Al) asymmetric stretching vibrations toward lower wavenumbers 968, 965, and 970 cm^{-1} for GPA, GPB, and GPC, respectively, in relation to the band at 989 cm^{-1} in MWFA and the formation of new crystalline phases. The pH effect showed electrostatic interactions as a significant adsorption mechanism. The Langmuir maximum adsorption capacities increased in the order 1.872, 15.899, 16.970, and 20.010 mg/g with increasing SS/SH mole ratios for MWFA, GPA (0.17), GPB (0.21), and GPC (0.24), respectively. The SS/SH of 0.24 produced an MWFA-based geopolymer with the highest adsorption capacity and performance. Alkalination of MWFA is shown to be a beneficial pre-treatment step both for the adsorption capacity and adsorption rate. The adsorbent–adsorbate affinity and adsorption rates were independent of the composition of the geopolymer. The sorption kinetics of endosulfan onto the geopolymers followed the pseudo-first-order kinetics, while the equilibrium data were best described by the Langmuir isotherm model. Thermodynamically, the adsorption processes were endothermic ($\Delta H > 0$), spontaneous ($\Delta G < 0$), physical, and entropy-driven.

Data availability statement

The data presented in the study is deposited in the Science data bank repository, accession number DOI 10.57760/sciencedb.07535. The authors confirm that the data has been deposited and is available at https://www.scidb.cn/anonymous/QU56cVlq.

Author contributions

Author contributions/credit IL, conceptualization, visualization, methodology, and writing—original draft. VS, conceptualization, methodology, writing—review and editing, supervision, and resource mobilization, including funding. DO, writing—review and editing, supervision, and characterization. BO, writing—review and editing and material characterization. CK, conceptualization, visualization, methodology, writing—review and editing, and supervision.

Funding

This work was funded by the Kaimosi Friends University Internal Research Grant [KAF/601/APPL/043/1(6)].

Acknowledgments

The authors would also like to thank Dr. Pierre Kalenga Mubiayi (University of the Witwatersrand, Johannesburg) for access to their research facilities.

Conflict of interest

The authors declare that the research was conducted in the absence of any commercial or financial relationships that could be construed as a potential conflict of interest.

Publisher's note

All claims expressed in this article are solely those of the authors and do not necessarily represent those of their

affiliated organizations, or those of the publisher, the editors, and the reviewers. Any product that may be evaluated in this article, or claim that may be made by its manufacturer, is not guaranteed or endorsed by the publisher.

Supplementary material

The Supplementary Material for this article can be found online at: https://www.frontiersin.org/articles/10.3389/fenvc.2023.1164372/full#supplementary-material

References

Al-Ghouti, M. A., Khan, M., Nasser, M. S., Al Saad, K., and Ee Heng, O. (2020). Application of geopolymers synthesized from incinerated municipal solid waste ashes for the removal of cationic dye from water. *Plos One J.* 15 (11), e0239095. doi:10.1371/journal.pone.0239095

Al-Samarai, G. F., Mahdi, W. M., and Al-Hilali, B. M. (2018). Reducing environmental pollution by chemical herbicides using natural plant derivatives – allelopathy effect. *Ann. Agric. Environ. Med. AAEM* 25 (3), 449–452. doi:10.26444/aaem/90888

Alacabey, I. (2022). Endosulfan elimination using amine-modified magnetic diatomite as an adsorbent. *Front. Chem.* 10, 907302. doi:10.3389/fchem.2022.907302

Craig, I. P., Bundschuh, J., and Thorpe, D. (2015). Pesticides sustainable management practice (SMP) including porous biochar/geopolymer structures for contaminated water remediation. *Int. J. GEOMATE* 9 (2), 1523–1527. https://geomatejournal.com/geomate/article/view/1841.

Daud, N. A. A., Shamsuddin, M. R., Pradanawati, S. A., and Rabat, N. E. (2021). Preparation, characterization and performance evaluation of fly ash-based composite geopolymer membranes for methylene blue dye removal. *Sci. Eng. Health Stud.* 15, 21020011. doi:10.14456/sehs.2021.38

Dzoujo, H. T., Shikuku, V. O., Tome, S., Akiri, S., Kengne, N. M., Abdpour, S., et al. (2022). Synthesis of pozzolan and sugarcane bagasse derived geopolymer-biochar composites for methylene blue sequestration from aqueous medium. *J. Environ. Manag.* 318 (4), 115533. doi:10.1016/j.jenvman.2022.115533

El Alouani, M., Alehyen, S., El Achouri, M., and Taibi, M. (2018). Removal of cationic dye- methylene blue-from aqueous solution by adsorption on fly ash-based geopolymer. *J. Mater. Environ. Sci.* 9 (1), 32–46. doi:10.26872/jmes.2018.9.1.5

Fabricius, A. L., Renner, M., Voss, M., Funk, M., Perfoll, A., Gehring, F., et al. (2020). Municipal waste incineration fly ashes: From a multi-element approach to market potential evaluation. *Environ. Sci. Eur.* 32, 88. doi:10.1186/s12302-020-00365-y

Freundlich, H. M. F. (1906). Über die adsorption in lösungen. *Z. fur Phys. Chem.* 57, 385–470. doi:10.1515/zpch-1907-5723

Ghani, U., Hussain, S., ul-Amin, N., Imtiaz, M., and Khan, S. A. (2020). Laterite clay-based geopolymer as a potential adsorbent for the heavy metals removal from aqueous solutions. *J. Saudi Chem. Soc.* 24 (11), 874–884. doi:10.1016/j.jscs.2020.09.004

Gupta, P., Nagpal, G., and Gupta, N. (2021). Fly ash based geopolymers: An emerging sustainable solution for heavy metal remediation from aqueous medium. *Beni-Suef Univ. J. Basic Appl. Sci.* 10, 89. doi:10.1186/s43088-021-00179-8

Gupta, V. K., and Imran, A. (2008). Removal of endosulfan and methoxychlor from water on carbon slurry. *Environ. Sci. Technol.* 42 (3), 766–770. doi:10.1021/es7025032

Halsey, G. (1948). Physical adsorption on non-uniform surfaces. *J. Chem. Phys.* 16, 931–937. doi:10.1063/1.1746689

Hengpraprom, S., Lee, C., and Coates, J. T. (2006). Sorption of humic acids and alpha-endosulfan by clay minerals. *Environ. Toxicol. Chem.* 25 (1), 11–17. doi:10.1897/05-119r.1

Hermann, D. T., Tome, S., Shikuku, V. O., Tchuigwa, J. T., Spieß, A., Janiak, C., et al. (2022). Enhanced performance of hydrogen peroxide modified pozzolan-based geopolymer for abatement of methylene blue from aqueous medium. *Silicon* 14, 5191–5206. doi:10.1007/s12633-021-01264-4

Ho, Y. S., and McKay, G. (1999). Pseudo-second order model for sorption processes. *Process Biochem.* 34 (5), 451–465. doi:10.1016/S0032-9592(98)00112-5

Hwang, J. I., Zimmerman, A. R., and Kim, J. E. (2018). Bioconcentration factor-based management of soil pesticide residues: Endosulfan uptake by carrot and potato plants. *Sci. total Environ.* 627, 514–522. doi:10.1016/j.scitotenv.2018.01.208

Innocenzi, P., Falcaro, P., Grosso, D., and Babonneau, F. (2003). Order-disorder transitions and evolution of silica structure in self-assembled mesostructured silica films studied through FTIR spectroscopy. *J. Phys. Chem. B* 107 (20), 4711–4717. doi:10.1021/jp026609z

Jemutai-Kimosop, S., Okello, V., Shikuku, V., Orata, F., and Getenga, Z. M. (2022). Synthesis of mesoporous akaganeite functionalized maize cob biochar for adsorptive abatement of carbamazepine: Kinetics, isotherms, and thermodynamics. *Clean. Mater.* 5, 100104. doi:10.1016/j.clema.2022.100104

Jiang, N., Shang, R., Heijman, S. G. J., and Rietveld, L. C. (2018). High-silica zeolites for adsorption of organic micro-pollutants in water treatment: A review. *A Rev. Water Res.* 144, 145–161. doi:10.1016/j.watres.2018.07.017

Kakoi, B., Kaluli, J. W., Thumbi, G., and Gachanja, A. (2015). Performance of activated carbon prepared from Sawdust as an adsorbent for endosulfan pesticide. *J. Sustain. Res. Eng.* 2 (1), 1–10.

Karaer, H., and Kaya, I. (2016). Synthesis, characterization of magnetic chitosan/active charcoal composite and using at the adsorption of methylene blue and reactive blue. *Microporous Mesoporous Mater.* 232, 26–38. doi:10.1016/j.micromeso.2016.06.006

Kegley, S. E., Hill, B. R., Orme, S., and Choi, A. H. (2010). *Pesticide action network pesticide database. Pesticide action Network*. San Francisco CA: North America.

Kughur, P. G. (2012). The effect of herbicides on crop production and environment in Makurdi local government area of Benue State, Nigeria. *J. Sustain. Dev. Afr.* 14 (4), 1520–5509. https://jsd-africa.com/Jsda/Vol14No4-Summer2012B/PDF/The%20Effects%20of%20Herbicides%20on%20Crop%20Production%20and%20Environment.Peter%20Gyanden%20Kughur.pdf.

Langmuir, I. (1918). The constitution and fundamental properties of solids and liquids. *J. Am. Chem. Soc.* 38, 2221–2295. doi:10.1021/ja02268a002

Liu, Y., He, Z., Shankle, M., and Tewolde, H. (2016). Compositional features of cotton plant biomass fractions characterized by attenuated total reflection Fourier transform infrared spectroscopy. *Industrial crops Prod.* 79, 283–286. doi:10.1016/j.indcrop.2015.11.022

Lubick, N. (2010). Endosulfan's exit: U.S. EPA pesticide review leads to a ban. *Science* 328 (5985), 1466. doi:10.1126/science.328.5985.1466

Maingi, F. M., Mbuvi, H. M., Ng'ang'a, M. M, and Mwang, H. (2017). Adsorption kinetics and isotherms of methylene blue by geopolymers derived from common clay and rice husk ash. *Phys. Chem.* 7 (4), 87–97. doi:10.5923/j.pc.20170704.02

Maleki, A., Hadizadeh, Z., Sharifi, V., and Emdadi, Z. (2019). A green, porous and eco-friendly magnetic geopolymer adsorbent for heavy metals removal from aqueous solutions. *J. Clean. Prod.* 215 (1), 1233–1245. doi:10.1016/j.jclepro.2019.01.084

Meroufel, B., Benali, O., Benyahia, M., Benmoussa, Y., and Zenasni, M. A. (2013). Adsorptive removal of anionic dye from aqueous solutions by Algerian kaolin: Characteristics, isotherm, kinetic and thermodynamic studies. *J. Mater. Environ. Sci.* 4 (3), 482–491. https://www.jmaterenvironsci.com/Document/vol4/vol4_N3/60-JMES-361-2013-Meroufel.pdf.

Mishra, T., and Tiwari, S. K. (2006). Studies on sorption properties of zeolite derived from Indian fly ash. *J. Hazard. Mater.* 137, 299–303. doi:10.1016/j.jhazmat.2006.02.004

Nath, P., and Sarker, P. (2017). Flexural strength and elastic modulus of ambient-cured blended low-calcium fly ash geopolymer concrete. *Constr. Build. Mater.* 130, 22–31. doi:10.1016/j.conbuildmat.2016.11.034

Patocka, J., Wu, Q., Franca, T. C. C., Ramalho, T. C., Pita, R., and Kuca, K. (2016). Clinical aspects of the poisoning by the pesticide endosulfan. *Quím. Nova* 39 (8), 987–994. doi:10.5935/0100-4042.20160102

Peydayesh, M., Isanejad, M., Mohammadi, T., and Jafari, S. M. R. S. (2015). Assessment of *urtica* as a low-cost adsorbent for methylene blue removal: Kinetic, equilibrium, and thermodynamic studies. *Chem. Papers- Slovak Acad. Sci.* 69, 930–937. doi:10.1515/chempap-2015-0097

Polati, S., Angioi, S., Gianotti, V., Gosetti, F., and Genarro, M. C. (2006). Sorption of pesticides on Kaolinite and Montmorillonite as a function of hydrophilicity. J. Environ. Sci. Health, *part B* 41 (4), 333–344. doi:10.1080/03601230600591416

Rauf, N., Tahir, S. S., Kang, J. H., and Chang, Y. S. (2012). Equilibrium, thermodynamics and kinetics studies for the removal of alpha and beta endosulfan by adsorption onto bentonite clay. *Chem. Eng. J.* 192, 369–376. doi:10.1016/j.cej.2012.03.047

Revellame, E. D., Fortela, D. L., Sharp, W., Hernandez, R., and Zappi, M. E. (2020). Adsorption kinetic modeling using pseudo-first order and pseudo-second order rate laws: A review. *Clean. Eng. Technol.* 1, 100032. doi:10.1016/j.clet.2020.100032

Roberts, E. M., English, P. B., Grether, J. K., Windham, G. C., Somberg, L., and Wolff, C. (2007). Maternal residence near agricultural pesticide applications and autism spectrum disorders among children in the California Central Valley. *Environ. Health Prospects* 115 (10), 1482–1489. doi:10.1289/ehp.10168

Sarkar, C., Basu, J. K., and Samanta, A. N. (2019). Experimental and kinetic study of fluoride adsorption by Ni and Zn modified LD slag based geopolymer. *Chem. Eng. Res. Des.* 142, 165–175. doi:10.1016/j.cherd.2018.12.006

Sarkar, C., Basu, J. K., and Samanta, A. N. (2017). Removal of Ni^{2+} ion from waste water by geopolymeric adsorbent derived from LD slag. *J. Water Process Eng.* 17, 237–244. doi:10.1016/j.jwpe.2017.04.012

Shikuku, V. O., and Kimosop, S. (2020). Efficient removal of sulfamethoxazole onto sugarcane bagasse-derived biochar: Two and Three-parameter isotherms, kinetics, thermodynamics. *South Afr. J. Chem.* 73, 111–118. doi:10.17159/0379-4350/2020/v73a16

Shikuku, V. O., Kowenje, C. O., and Kengara, F. (2018). Errors in parameters estimation using linearized adsorption isotherms: Sulfadimethoxine adsorption onto kaolinite clay. *Chem. Sci. Inter. J.* 23, 1–6. doi:10.9734/csji/2018/44087

Shikuku, V. O., and Sylvain, T. (2019). "Application of geopolymer composites in wastewater treatment: Trends, opportunities, and challenges," in *Polymer nanocomposites for advanced engineering and military applications*. Editor N. Ramdani (Pennsylvania, United States: (IGI Global), 131–149. doi:10.4018/978-1-5225-7838-3.ch005

Shikuku, V. O., Tome, S., Dzoujo, T. H., Thompsett, G. A., and Timko, M. T. (2022). Rapid Adsorption of Cationic Methylene Blue dye onto volcanic ash-metakaolin based geopolymers. *Silicon* 14, 9349–9359. doi:10.1007/s12633-021-01637-9

Shikuku, V. O., Zanella, R., Kowenje, C. O., Donato, F. F., Bandeira, N. M. G., and Prestes, O. D. (2018). Single and binary adsorption of sulfonamide antibiotics onto iron-modified clay: Linear and nonlinear isotherms, kinetics, thermodynamics, and mechanistic studies. *Appl. Water Sci.* 8, 175. doi:10.1007/s13201-018-0825-4

Shokrollahi, A., Alizadeh, A., Malekhosseini, Z., and Ranjbar, M. (2011). Removal of bromocresol green from aqueous solution via adsorption on ziziphus nummularia as a new, natural, and low-cost adsorbent: Kinetic and thermodynamic study of removal process. *J. Chem. Eng. Data* 15, 3738–3746. doi:10.1021/je200311y

Sipes, N. S., Martin, M. T., Kothiya, P., Reif, D. M., Judson, R. S., Richard, A. M., et al. (2013). Profiling 976 ToxCast chemicals across 331 enzymatic and receptor signaling assays. *Chem. Res. Toxicol.* 26 (6), 878–895. doi:10.1021/tx400021f

Siyal, A. A., Azizli, K. A., Man, Z., and Ullah, H. (2016). Effects of parameters on the setting time of fly ash based geopolymers using Taguchi method, http://creativecommons.org/licences/by-nc-nd/4.0/. *Procedia Eng.* 148, 302–307. doi:10.1016/j.proeng.2016.06.624

Siyal, A. A., Shamsuddin, M. R., Khan, M. I., Rabat, N. E., Zulfiqar, M., Man, Z., et al. (2019). Fly ash based geopolymer for the adsorption of anionic surfactant from aqueous solution. *J. Clean. Prod.* 229, 232–243. doi:10.1016/j.jclepro.2019.04.384

Siyal, A. A., Shamsuddin, M. R., Khan, M. I., Rabat, N. E., Zulfiqar, M., Man, Z., et al. (2018). A review on geopolymers as emerging materials for the adsorption of heavy metals and dyes. *J. Environ. Manag.* 224, 327–339. doi:10.1016/j.jenvman.2018.07.046

Sudhakar, Y., and Dikshit, A. K. (1999). Adsorbent selection for endosulfan removal from water environment. *J. Environ. Sci. Health, Part B* 34 (1), 97–118. doi:10.1080/03601239909373186

Tome, S., Dzoujo, T. H., Shikuku, V. O., and Otieno, S. (2021). Synthesis, characterization and application of acid and alkaline activated volcanic ash-based geopolymers for adsorptive remotion of cationic and anionic dyes from water. *Ceram. Int.* 47 (15), 20965–20973. doi:10.1016/j.ceramint.2021.04.097

Tome, S., Etoh, M.-A., Etame, J., and Sanjay, K. (2018). Characterization and leachability behaviour of geopolymer cement synthesised from municipal solid waste incinerator fly ash and volcanic ash blends. *Recycling* 3 (4), 50. doi:10.3390/recycling3040050

Treybal, R. E. (1980). *Mass transfer operations*. 3rd edn. New York, USA: McGraw-Hill.

Yedla, S., and Dikshit, A. (2008). Removal of Endosulfan from Water Using Wood Charcoal-Adsorption and Desorption. *Journal of Environmental Engineering-asce - J ENVIRON ENG-ASCE* 134 (2), 102–109. doi:10.1061/(asce)0733-9372(2008)134:2(102)

Yonli, A. H., Batonneau-Gener, I., and Koulidiati, J. (2012). Adsorptive removal of α-endosulfan from water by hydrophobic zeolites. An isothermal study. *J. Hazard. Mater.* 203, 357–362. doi:10.1016/j.jhazmat.2011.12.042

Yuh-Shan, H. (2004). Citation review of lagergren kinetic rate equation on adsorption reactions. *Scientometrics* 59 (1), 171–177. doi:10.1023/B:SCIE.0000013305.99473.cf

Zhang, Z., Yao, X., and Wang, H. (2012). Potential application of geopolymers as protection coatings for marine concrete III. Field experiment. *Appl. Clay Sci.* 67, 57–60. doi:10.1016/j.clay.2012.05.008

Zió lkowska, D., Shyichuk, A., Karwasz, I., and Witkowska, M. (2009). Adsorption of cationic and anionic dyes onto commercial kaolin. *Adsorpt. Sci. Technol.* 27 (2), 205–214. doi:10.1260/026361709789625306

Zulkifly, K., Yong, H. C., Abdullah, M. M. B., Ming, L. Y., Sandu, A. V., and Abdullah, S. F. A. (2019). Characterization of fly ash and metakaolin blend geopolymers under ambient temperature condition. *Mater. Sci. Eng.* 551, 012086. doi:10.1088/1757-899X/551/1/012086